European Journal of Medicinal Chemistry 59 (2013) 235–242

Contents lists available at SciVerse ScienceDirect

European Journal of Medicinal Chemistry

journal homepage: http://www.elsevier.com/locate/ejmech

Original article

Selective and potent adenosine A_3 receptor antagonists by methoxyaryl substitution on the *N*-(2,6-diarylpyrimidin-4-yl)acetamide scaffold

Vicente Yaziji [a,b], David Rodríguez [d], Alberto Coelho [a,b], Xerardo García-Mera [c], Abdelaziz El Maatougui [a,b], José Brea [b], María Isabel Loza [b], María Isabel Cadavid [b], Hugo Gutiérrez-de-Terán [d,**], Eddy Sotelo [a,b,c,*]

[a] Combinatorial Chemistry Unit (COMBIOMED), Center for Research in Biological Chemistry and Molecular Materials (CIQUS), University of Santiago de Compostela, 15782, Spain
[b] Institute of Industrial Pharmacy, University of Santiago de Compostela, 15782, Spain
[c] Department of Organic Chemistry, Faculty of Pharmacy, University of Santiago de Compostela, 15782, Spain
[d] Public Galician Foundation of Genomic Medicine, Santiago de Compostela University Hospital (CHUS), 15706 Santiago de Compostela, Spain

ARTICLE INFO

Article history:
Received 24 September 2012
Received in revised form
6 November 2012
Accepted 8 November 2012
Available online 24 November 2012

Keywords:
Adenosine receptor
3D-QSAR
Grid-Independent Descriptors (GRIND-2)
Suzuki–Miyaura cross-coupling reaction
Pyrimidines
Adenosine antagonists
Library synthesis

ABSTRACT

The influence of diverse methoxyphenyl substitution patterns on the *N*-(2,6-diarylpyrimidin-4-yl)acetamide scaffold is herein explored in order to modulate the A_3 adenosine receptor antagonistic profile. As a result, novel ligands exhibiting excellent potency (K_i on A_3 AR < 20 nM) and selectivity profiles (above 100-fold within the adenosine receptors family) are reported. Moreover, our joint theoretical and experimental approach allows the identification of novel pharmacophoric elements conferring A_3AR selectivity, first established by a robust computational model and thereafter characterizing the most salient features of the structure–activity and structure–selectivity relationships in this series.

1. Introduction

The purine nucleoside adenosine exerts its key regulatory roles on several tissues through activation of the four adenosine receptors (ARs), namely A_1, A_{2A}, A_{2B} and A_3 [1]. Being members of the superfamily of G protein-coupled receptors (GPCRs), ARs are validated targets for pharmacological intervention in several pathophysiological conditions [2]. In addition, the crystallization of the human A_{2A}AR [3] is boosting the rational design of novel selective ligands for the different ARs. Among the ARs, A_3ARs are the latest cloned and pharmacologically characterized. The A_3AR is involved in a variety of important physiological processes, including modulation of cerebral and cardiac ischemic damage [4,5], inflammation [6], modulation of intraocular pressure [7], regulation of normal and tumor cell growth [8,9] and immunosuppression [10]. However, A_3-signaling in several processes is still controversial [11,12], being perhaps the most enigmatic among adenosine receptors. The two personalities of A_3AR often come into direct conflict, e.g., in ischemia, inflammation and cancer, rendering this receptor as a single entity behaving in 2 different ways. Thus, the elucidation of A_3AR dual behavior in several pathophysiological conditions remains an unmet challenge.

The antagonists of the A_3AR [13–15] have shown to be particularly attractive as novel potential anti-inflammatory drugs [6], cerebro-protective agents [16], as well as for the treatment of glaucoma [17]. Furthermore, the recent evidence of high expression levels of A_3AR in several cell lines has suggested potential applications in cancer chemotherapy [18]. The putative applications of A_3AR antagonists as drugs, as well as the growing demand for pharmacological tools to study the dual roles of human A_3AR, has made the identification of potent and selective small molecule ligands a topic of great interest [1,2,19]. The pursuit of non-

Abbreviations: ARs, human adenosine receptors; GPCRs, G protein-coupled receptors; 3D-QSAR, three-dimensional quantitative structure–activity relationships; GRIND2, GRid INdependent Descriptors version 2; MIF, molecular interaction fields.

* Corresponding author. Combinatorial Chemistry Unit (COMBIOMED), Center for Research in Biological Chemistry and Molecular Materials (CIQUS), University of Santiago de Compostela, 15782, Spain. Tel.: +34 881815732; fax: +34 881815704.
** Corresponding author. Tel.: +34 881815428; fax: +34 981951473.
E-mail addresses: hugo.teran@usc.es (H. Gutiérrez-de-Terán), e.sotelo@usc.es (E. Sotelo).

0223-5234/$ – see front matter © 2012 Elsevier Masson SAS. All rights reserved.
http://dx.doi.org/10.1016/j.ejmech.2012.11.010

xanthinic A_3AR antagonists focused on the exploration of diverse heterocyclic libraries (particularly tri- and bi-cyclic heteroaromatic scaffolds and, to a lesser extent, mono-heterocyclic systems). Whereas the systematic structural elaboration of these prototypes has provided derivatives possessing good affinity, the selectivity issue and the relatively poor bioavailability profiles of drug candidates have remained elusive until recently [1,2,19].

We have recently described highly potent and selective A_3AR antagonists through a straightforward and convergent synthetic pathway [20], obtaining single ringed heterocyclic cores showing low nanomolar affinities at the A_3AR and marked selectivity versus the other ARs. These molecules were designed by the structural redecoration of the aryl moieties at positions 2 and 6 of the *N*-(pyrimidin-4-yl)-acylamide scaffold [21], a fruitful substructure that is present in diverse ARs antagonists [2,21,22]. It was observed that the methoxy substituents on the phenyl ring not only increased the affinities for the hA_3AR, but also remarkably enhanced the selectivity profiles of this series (Fig. 1). This finding reinforces key observations from other authors [22–25], and motivated a thorough exploration of the pharmacological insights of methoxyaryl substitution patterns on the A_3AR antagonistic profile of *N*-(2,6-diphenylpyrimidin-4-yl) acetamides. Building upon the development of a computational model with satisfactory predictivity together with an efficient and flexible synthetic methodology, we herein report the design, synthesis and pharmacological evaluation of an expanded series derived from the *N*-(2,6-diphenylpyrimidin-4-yl)acetamide scaffold. This study, in addition to providing novel potent A_3AR antagonists, highlights several novel methoxyphenyl-derived pharmacophoric elements conferring A_3AR selectivity, as well as the most salient features of the structure–activity (SAR) and structure–selectivity (SSR) relationships in this series.

2. Molecular modeling

A small library consisting of ten *N*-[(2,6-bisaryl)pyrimidin-4-yl]-acetamides was designed, including mono-, bi- and trimethoxyphenyl substitution patterns as well as 4-ethoxyphenyl, 4-trifluoromethoxyphenyl and 4-methoxystyryl residues. The designed molecules were then evaluated *in silico*, using combined Structure- and Ligand-Based computational pipeline protocol derived from our previous work [20], which is here adapted as summarized in Fig. 2. Briefly, the protocol includes two stages:

(i) Molecular docking of each ligand on a homology model of the hA_3AR, built with MODELLER [26] using the inactive structure of $A_{2A}AR$ (PDB code 3EML) [3] as a template. The program GOLD [27] was employed with the parameters indicated in the Experimental Section, and the observed poses were compared with the consensus binding mode defined for this scaffold [20].

(ii) 3D-QSAR: In parallel to the docking studies, a predictive 3D-QSAR model was built using the 68 molecules with previously reported K_i values [20], by means of the last generation of Grid-Independent Descriptors (GRIND-2) [28]. The software Pentacle [29] was used for this purpose, with the parameters detailed in the Experimental Section. Thereafter, the relative affinities of the filtered compounds (those that achieved the conserved binding orientation discussed below) were evaluated with the 3D-QSAR *model II* (see Table 1), using the "Prediction mode" included in Pentacle. The interpretation of QSAR models developed with the GRIND-2 methodology is based on the analysis of the correlograms, which encode the geometrical relationships between the most relevant molecular interaction fields (MIFs). Thereafter, one can easily

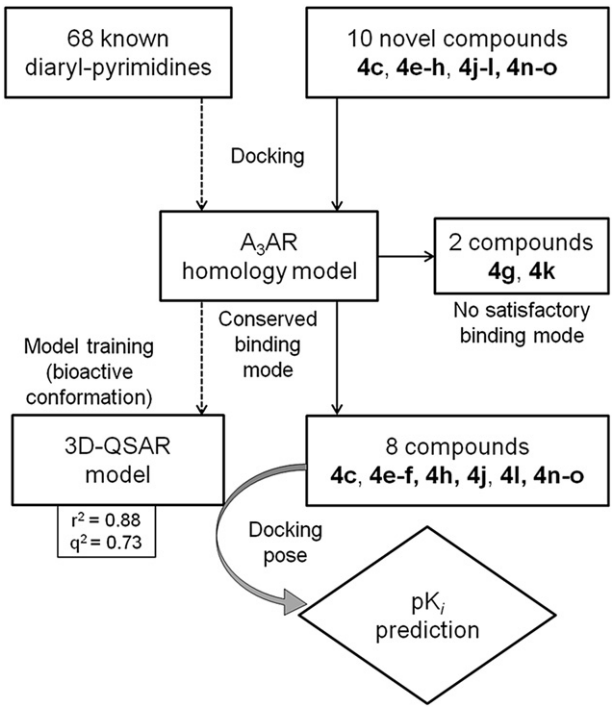

Fig. 2. Combined structure- and ligand-based computational protocol for the affinity prediction of novel compounds in A_3AR.

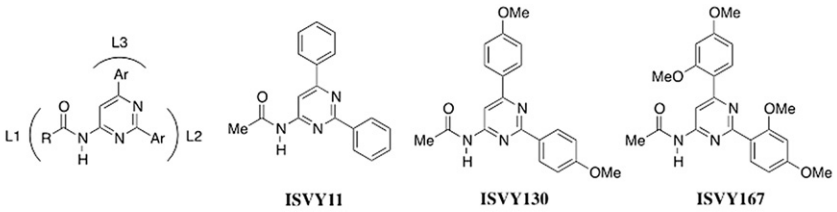

Code	hA_1¥	hA_{2A}¥	hA_{2B}¥	hA_3¥
ISVY11	31.20	255.30	19%	12.10
ISVY130	1%	10%	4%	3.60 ± 0.2
ISVY167	1%	6%	2%	5.40 ± 0.1

¥ Adenosine binding data is expressed as Ki (nM) or as % of displacement at 0.1 μM

Fig. 1. The *N*-[(2,6-bisaryl)pyrimidin-4-yl]-acetamide scaffold and the effect on the selectivity profile of the (poly)methoxy substitution on the phenyl fragments. The substitutions follow the nomenclature of an A_1AR model [10].

Table 1
Summary of 3D-QSAR models considered in this work. The number of molecules and latent variables considered for each model are indicated, as well as statistics regarding their accuracy and predictivity in cross-validation. Prospective assessment is also shown where applicable, with the number of new molecules evaluated and the standard deviation (in pK_i units) of their corresponding predictions.

Model	Cpds.	LV	R2	Q2	SDEP	SDEC	New cpds. pred.	SDEP pred.
I[a]	62	2	0.86	0.67	0.48	0.31	6	0.37
II[b]	68	2	0.88	0.73	0.42	0.29	8[c]	0.73[c]
III[d]	76	3	0.88	0.70	0.44	0.28	–	–

[a] Model built with 62 diaryl-pyrimidines, see Ref. [9].
[b] Model elaborated with both the training and tested molecules in *model I*.
[c] All the novel molecules presented in this work that found a satisfactory docking binding mode on a homology model of A_3AR. Note that the elimination of compound **4e** would diminish the value of the SDEP to 0.49 pK_i units, which is close to the SDEP of the internal validation of the model itself.
[d] Partial least squares 3D-QSAR model generated with the molecules present in *model II* plus the novel 8 compounds.

identify and further examine the pharmacophoric variables that contribute the most to the partial least squares fitness, and thus to the modulation of the A_3AR affinity.

3. Chemistry

Guided by the modeling results, we assembled a focused library that was representative of the diverse substitution patterns on the phenyl residues of the *N*(2,6-diphenylpyrimidin-4-yl)-acetamide template. The synthetic pathway developed follows a two-step sequence as illustrated in Scheme 1 [30]. The selected approach is based on the highly reliable and well-established Suzuki–Miyaura cross-coupling reaction [31], exploiting the excellent commercial availability of boronic acids (**3**). Acetylation of the heterocyclic core and subsequent palladium-catalyzed arylation afforded a library of fifteen *N*-(2,6-diphenylpyrimidin-4-yl)acetamides (**4a**–**o**) in yields ranging 73–91%.

4. Pharmacology

The pharmacological profile of the synthesized compounds (**4a**–**o**) was studied *in vitro* at the four human adenosine receptor subtypes, using radioligand binding assays according to the experimental protocols described elsewhere [32]. Table 2 compiles the pharmacological data, together with the associated computational predictions, obtained for the 10 novel compounds here presented: **4c**, **4e**–**h**, **4j**–**l** and **4n**–**o**. For comparative purposes, some derivatives previously described by our group [20] (**4a**, **4b**, **4d**, **4i** and **4m**) were evaluated again and incorporated into the series.

5. Results and discussion

The consensus binding mode proposed for the *N*-[(2,6-bisaryl) pyrimidin-4-yl]acetamide scaffold is illustrated in Fig. 3A [9]. From the 10 novel ligands, 8 presented this conserved binding mode, which is defined by a double hydrogen bond of the exocyclic amido

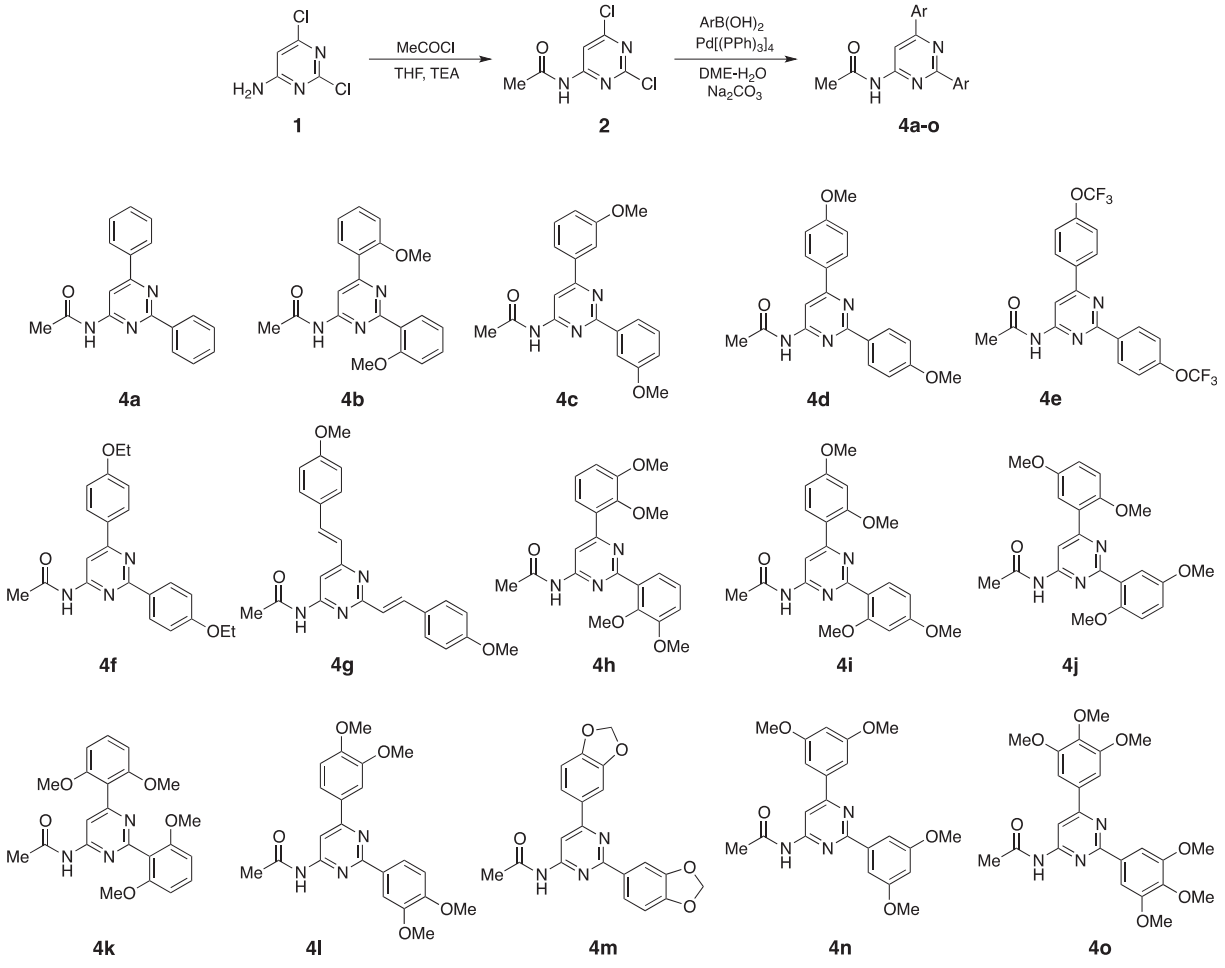

Scheme 1. Synthetic pathway and structure of the compounds here presented (**4a**–**o**).

Table 2
Structure and affinity data for the *N*-(2,6-diarylpyrimidin-4-yl)acetamides (**4a**–**o**) at the human adenosine receptors.

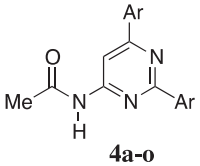

4a-o

Comp	Ar	K_i (nM) or % at 1 μM				pK_i @ hA_3	
		hA_1[a]	hA_{2A}[b]	hA_{2B}[c]	hA_3[d]	Exp	Pred[e]
4a[f]	Ph	31.2 ± 4.1	255.3 ± 1.3	22%	12.1 ± 1.3	7.92	*7.83*
4b[f] (**ISVY158**)	2-OMe-Ph	4%	15%	7%	24.1 ± 1.3	7.62	*7.43*
4c	3-OMe-Ph	22.6 ± 2.4	49.4 ± 3.7	67.5 ± 4.3	2.8 ± 0.1	8.55	8.26
4d[f] **(ISVY130)**	4-OMe-Ph	2%	4%	2%	3.6 ± 0.2	8.44	*8.32*
4e	4-OCF_3-Ph	8%	1%	4%	389.0 ± 8.5	6.41	8.02
4f	4-OEt-Ph	12%	2%	1%	40.2 ± 2.6	7.40	8.06
4g	4-OMe-Styryl	16%	13%	2%	513.1 ± 9.8	6.29	n.p.
4h	2,3-OMe-Ph	10%	375.1 ± 8.3	493.7 ± 5.1	42.4 ± 2.2	7.37	7.43
4i[f] **(ISVY167)**	2,4-OMe-Ph	3%	10%	7%	5.4 ± 0.1	8.27	*8.25*
4j **(ISVY350)**	2,5-OMe-Ph	4%	17%	1%	6.3 ± 0.3	8.20	7.85
4k	2,6-OMe-Ph	4%	1%	3%	4%	–	n.p.
4l **(ISVY345)**	3,4-OMe-Ph	10%	5%	2%	5.2 ± 0.2	8.28	8.19
4m[f]	3,4-OCH_2O-Ph	17.00 ± 3.1	3345.0 ± 1127	6%	3.3 ± 0.4	8.48	*8.11*
4n	3,5-OMe-Ph	15%	3%	1%	55.0 ± 3.1	7.26	8.15
4o	3,4,5-OMe-Ph	14%	1%	1%	26.1 ± 2.1	7.58	8.04

[a] Displacement of specific [^{3}H]DPCPX binding in human CHO cells expressed as K_i ± SEM in nM ($n = 3$) or percentage displacement of specific binding at a concentration of 1 μM ($n = 2$).
[b] Displacement of specific [^{3}H]4-(2-[7-Amino-2-(2-furyl) [1,2,4]triazolo[2,3-*a*] [1,3,5]triazin-5-ylamino]ethyl)phenol binding in human HeLa cells expressed as K_i ± SEM in nM ($n = 3$) or percentage displacement of specific binding at a concentration of 1 μM ($n = 2$).
[c] Displacement of specific [^{3}H]DPCPX binding in human HEK-293 cells expressed as K_i ± SEM in nM ($n = 3$) or percentage displacement of specific binding at a concentration of 1 μM ($n = 2$).
[d] Displacement of specific [^{3}H]NECA binding in human HeLa cells expressed as K_i ± SEM in nM ($n = 3$) or percentage displacement of specific binding at a concentration of 1 μM ($n = 2$).
[e] Ligands **4g** and **4k** are marked as not predicted (n.p.), since they do not present the conserved binding mode in the molecular docking stage.
[f] For comparative purposes, previously described compounds (Ref. [9]) were evaluated again at 1 μM, these compounds were included in the generation of the 3D-QSAR model, thus the calculated pK_i value on A_3AR is indicated in italics.

group (donating) and the N3 of the heterocyclic core (accepting) with Asn 6.55 (note Ballesteros & Weinstein numbering [33]), plus a δ stacking interaction with Phe 5.29 at EL2. In addition to these interactions with the abovementioned residues, which are totally conserved in the ARs family, the binding of the central heterocycle is reinforced by hydrophobic interactions with Leu 6.51 (see Fig. 3A). The symmetric aryl substitutions are accommodated respectively within the binding pocket defined by Leu 3.32, *Ser 5.42*, *Ser 6.52* and Trp 6.48 (substituent L2) and Val 2.64, Leu 3.33 and Leu 7.35 (substituent L3), the residues in italics being specific for the A_3AR. The release of a new crystal structure of the A_{2A}AR (also in its inactive conformation) with a 1,2,4-triazine derivative [34], an antagonist that shows a relative chemical similarity to our scaffold, provided us the opportunity of further assessing this binding orientation. This comparison is illustrated in Fig. 3B, and provides an experimental support to the binding mode discussed for our *N*-[(2,6-bisaryl)pyrimidin-4-yl]-acetamide scaffold. Once defined the binding orientation, and following the protocol in Fig. 1, the 8 ligands selected in the docking stage were evaluated in a 3D-QSAR model. Such a model had been built with a training set of 68 molecules previously reported by us (*model II* in Table 1), presenting very good accuracy ($r^2 = 0.88$) and predictivity ($q^2 = 0.73$) in the leave-one-out cross-validation. The predictions for the selected 8 compounds anticipated high affinities for all of them, in the range of 7.43–8.26 pK_i units.

The experimental binding affinities confirm that most of the examined compounds display high affinities for the hA_3AR, in the nanomolar range (Table 2), being particularly noteworthy some novel, highly potent and selective ligands (e.g., compounds **4j**, **4l**, **4f**, **4n**). Moreover, the predictions of the computational model show good agreement with the experimental results (Table 2 and Fig. 4A). The two compounds that did not achieve the consensus binding orientation in the docking stage (**4g** and **4k**) were experimentally confirmed as the weakest binders within the whole series. Compound **4g**, that can hardly accommodate the 4-OMe-styryl substituents in the binding site, exhibit a reduced A_3AR affinity ($pK_i < 6.5$). Similarly, the highly restrained conformational spectrum of compound **4k** (due to the 2,6-dimethoxy substitution pattern) probably precludes its binding to any AR. The predictions of the 3D-QSAR model for the 8 new molecules (**4c**, **4e**–**f**, **4h**, **4j**, **4l** and **4n**–**o**) show an initial standard error of the prediction (SDEP) of 0.73 pK_i units. A closer examination revealed that approximately 1/3 of this error is due to the insensitivity of the model to the ~100 fold decrease in affinity of 4-trifuoromethoxyphenyl derivative **4e**, as compared to the related 4-methoxyphenyl compound **4d** (**ISVY130**) (see Table 2). Indeed, a similar detrimental effect of the trifluoro substitution was already observed in previous series [20], where the 4-trifluorotolyl derivative showed a 28-fold reduction in affinity as compared with the 4-tolyl compound (**ISVY133**).

In order to provide further interpretation of the structure–activity relationships of the series, a new 3D-QSAR model was generated now adding the novel 8 compounds to the training set of 68 compounds initially considered. The statistics of this refined model, (*model III* in Table 1), remain almost unchanged as

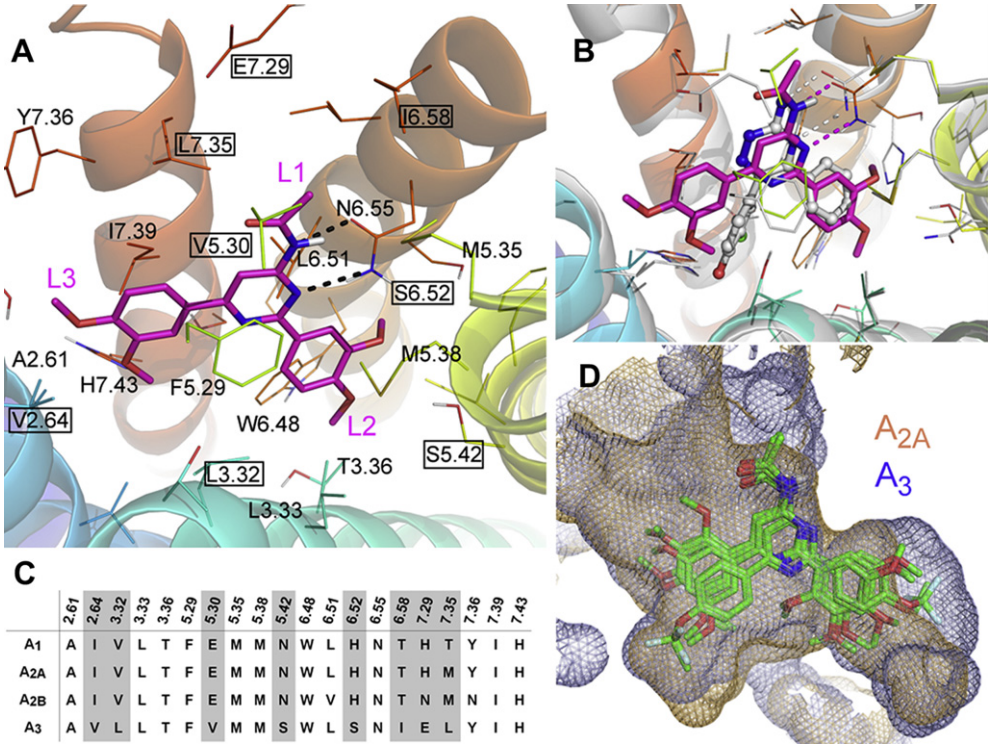

Fig. 3. Binding mode of novel compounds in A_3AR and selectivity considerations within ARs. (A) Docking pose of compound **4l** (**ISVY345**) in A_3AR: residues within 3 Å of the ligand are labeled, indicating with a square A_3AR specific residues. (B) Docking solution of panel A superimposed to X-ray structure of A_{2A}AR in complex with the 1,2,4-triazine derivative T4E (white carbons, PDB 3UZC). Both ligands present similar chemical scaffolds, and show common anchoring points with each receptor, while the aryl substituents sit in analogous binding subpockets. (C) Pseudo-sequence alignment the human ARs, including the binding site residues defined above, with the specific A_3AR residues shadowed in gray. (D) Docking poses of the novel compounds (**4c**, **4e**–**h**, **4j**–**l**, **4n**–**o**) in A_3AR, showing a superposition of the broader binding site surface of the A_3AR (blue) and that of the A_{2A}AR (orange, PDB 3EML). (For interpretation of the references to color in this figure legend, the reader is referred to the web version of this article.)

compared to previous models (see Table 1), thus adding confidence on the robustness of the 3D-QSAR methodology. The most important features identified by the model are illustrated in Fig. 4B and can be briefly summarized as follows: (*i*) the optimal substitution at the L1 site by an acetamide [TIP–TIP representing the alkyl substitutions at L1 at the optimal distance of 3 Á; TIP–N1 cross-correlogram delimiting the optimal distance (5 Á) between the surface of L1 and the interaction with Asn 6.55] and (*ii*) the relative disposition of the aromatic L2 and L3 substituents with respect to the surface tip of L1 (DRY-TIP cross-correlogram at an optimum distance of 13 Á). These features reinforce the initial interpretation of the interdependence of the size of L1 and L2/L3 substituents,

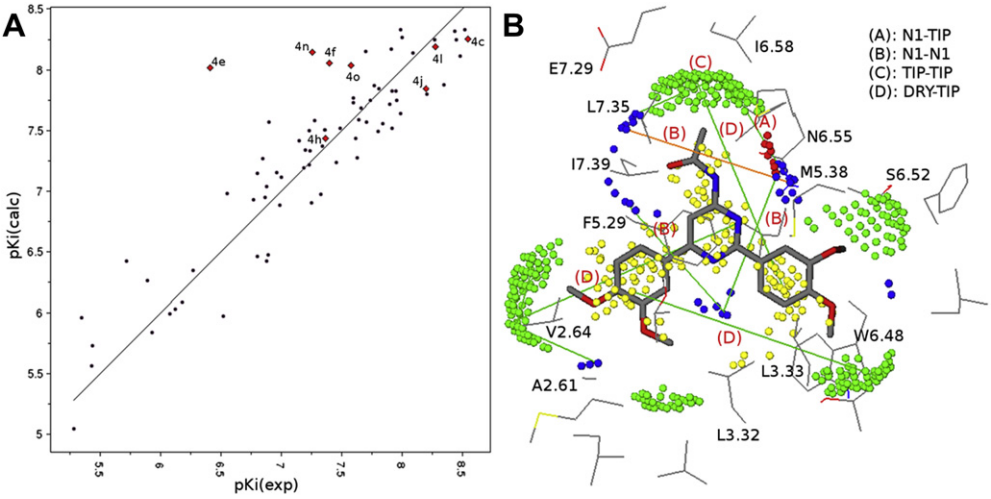

Fig. 4. Results of the 3D-QSAR modeling. (**A**) Representation of the experimental versus calculated affinities using the 3D-QSAR *model II* (see Table 1). Red diamonds represent newly predicted molecules by that model. **(B)** Most relevant correlogram vectors in the explanatory model (*model III* in Table 1) are represented for compound ISVY345 (**4l**) in the binding site of A_3AR, where main residues are labeled. The GRID nodes are represented by dots colored in yellow (DRY probe), blue (N1), red (O) and green (TIP). The main four vectors (N1–TIP, N1–N1, TIP–TIP and DRY–TIP) are labeled in red. (For interpretation of the references to color in this figure legend, the reader is referred to the web version of this article.)

which is optimally achieved with the acetamide in L1 and particularly 3 and 4 methoxy-phenyl substituents, i.e., compounds **4c**, **4d**, **4i**, **4j**, **4l** and the piperonyl derivative **4m**.

A comparison of the pharmacological data obtained for the parent compound of the series (**4a**, Ar = Ph, a potent but not selective ligand) and its mono-methoxy derivatives (*ortho* **4b**, *meta* **4c** and *para* **4d**) reveals a significant, but differentiated variation in their pharmacological profile. On one side, the introduction of the methoxy group at either *ortho* or *para* positions generated highly potent and completely selective ligands (**4b** and **4d**), with the 4-methoxyphenyl derivative (**4d**, K_i = 3.6 nM) displaying a 7-fold higher affinity than the 2-methoxyphenyl ligand **4b** (K_i = 24.1 nM). On the other side, methoxylation at position 3 afforded a ligand exhibiting an outstanding potency (**4c**, K_i = 2.8 nM), albeit reproducing the promiscuity profile of the parent compound (**4a**). Three novel compounds (**4e-g**) were synthesized on the basis of the optimal potency/selectivity profile observed for the 4-methoxyphenyl derivative **4d** [9], also encouraged by the predictions of the computational model (Table 2 and Fig. 4A). Even if compound **4g** was anticipated to hardly bind to the A_3AR model in the docking stage, we prepared and tested this styryl derivative to provide a broader characterization of the series and to further challenge the computational pipeline. While substitutions at the *para* position significantly attenuated the potency by 10–140 fold, these compounds retained an excellent selectivity profile, with the 4-ethoxyphenyl derivative **4f** displaying a satisfactory balance between moderate potency (K_i = 40.2 nM) and high selectivity. A complementary docking exploration in the A_{2A}AR crystal structure was performed to obtain deeper knowledge on the selectivity issues, as detailed in the Experimental Section. Encouragingly, only compounds with sub-micromolar affinity on A_{2A}AR (**4a**, **4c**, **4h**) achieve the conserved binding mode depicted for the A_3AR in Fig. 3, with the only exception of the 2-OMe-Ph substituted compound **4b**, a highly selective compound that also finds this conserved pose in A_{2A}R. According to this finding, the enhanced selectivity of the 4-substituted compounds (**4d**–**g**, as well as **4l**) could be explained by the lack of this binding orientation due to steric clashes with His 6.52 and Asn 5.42. Instead, A_3AR presents a smaller serine in the two equivalent positions, offering a bigger cavity to accommodate the *para* substitutions in the aromatic ring at L2. Fig. 3D shows the superposition of the binding site surface of the A_3AR (blue) and A_{2A}AR (orange), where it can be appreciated an increased surface to accommodate bulkier substituents, particularly at *meta* and *para* positions of the L2 moiety for binding A_3AR.

In an attempt to establish the optimum substitution patterns for the possible dimethoxyphenyl (2,3-, 2,4-, 2,5-, 2,6-, 3,4- and 3,5-), as well as trimethoxyphenyl derivatives, compounds **4h-o** were prepared and evaluated. A second methoxy group on the phenyl rings led to the identification of very potent (low nanomolar affinity) and completely selective ligands (e.g., compounds **4i**, **4j**, **4l**). The first remarkable observation is the ability of the 4-methoxyphenyl substitution to accommodate a second methoxy group in either *ortho* (**4i**) or *meta* (**4l**) without affecting the affinity and selectivity of the reference monosubstituted compound (**4d**). Even the 3,4,5-trimethoxyphenyl (**4o**) retains this high selectivity profile, while experiencing a less than 10- and 5-fold drop in A_3AR affinity, as compared to the mono (**4d**) or dimethoxyphenyl (**4l**) analogs respectively. Not surprisingly, compound **4o** displays an intermediate affinity when compared to the 3,4- (**4l**) and 3,5-dimethoxyphenyl (**4n**) analogs. The fact that all these bi- and tri-substituted compounds retain an excellent selectivity profile is again in agreement with the deeper subpocket identified for these voluminous substitutions at L2 in the A_3AR, as compared to other AR subtypes (see Fig. 3). Indeed, the limited selectivity observed for the piperonyl analog **4m**, which on the other side retains the affinity of the closest compound **4l** (K_i = 3.3 nM), may be explained by the reduced volume that the piperonyl residue can explore compared with the 3,4-OMe-Ph derivative (**4l**).

The SAR and SSR analysis for the remaining ligands can be discussed using the 2-methoxyphenyl derivative **4b** as reference. This ligand is a relatively potent (K_i = 24.1 nM) and highly selective hA_3AR antagonist, and a pairwise comparison of this compound with the dimethoxyphenyl derivatives that retain the *ortho*-methoxyphenyl (**4h-4k**) is especially suitable. The 2,4-dimethoxyphenyl (**4i**) and 2,5-dimethoxyphenyl (**4j**) congeners elicited remarkable affinity (K_i of 5.4 and 6.3 nM respectively) and selectivity for the A_3 receptor. As observed in the binding poses of these compounds on the A_3AR, depicted in Fig. 3D, the *ortho*-methoxy at L2 is preferably located close to the N1 of the pyrimidine ring, in a way that the *para* and *meta* methoxy groups in **4i** and **4j**, respectively, exploits the selective A_3AR subpocket defined by Ser 5.42 and Ser 6.52, discussed above. The 2,3-dimethoxyphenyl derivative **4h** can be compared with the monosubstituted derivatives in *ortho* (**4b**) and *meta* (**4c**), since it exhibits a slightly lower affinity for A_3 as compared to **4b**, while reproducing the non-selective profile observed for **4c**. Interestingly, the docking pose of this ligand places the *meta*-methoxy of L2 in the most buried area (i.e., closer to the N1 of the pyrimidine), as opposed to the selective A_3AR subpocket explored by 2,5-OMe-Ph (**4j**). This could explain the lower selectivity of the ligand **4h**, and also the meta monosubstituted derivative (**4c**), which according to the docking simulations adapts its binding pose to exploit the selective A_3AR subpocket while avoiding this region in A_{2A}AR, a differential binding mechanism probably occurring for the remaining ARs.

6. Conclusion

In summary, we have documented a comprehensive exploration of the *N*-(2,6-diarylpyrymidin-4-yl)acetamide scaffold with several combinations of methoxyphenyl residues at positions 2 and 6 of the heterocyclic core, reporting a series of novel optimized potent and selective A_3AR antagonists. The design of the current series was guided by our mixed structure-based/3D-QSAR computational pipeline, which not only demonstrated a good predictive power, but also shown its utility for interpreting the biological data here reported concerning the four human ARs. Two new molecules are particularly promising, **4j** (**ISVY350**) and **4l** (**ISVY345**), which combine excellent affinities for the hA_3AR ($K_i \leq 7$ nM) and highly selective profiles among ARs.

7. Experimental protocols

7.1. Computational methods

7.1.1. Structure-based methods: receptor preparation and ligand docking

Several programs and servers were employed for the generation of the homology model of A_3AR as originally reported in ref. [20]. These include (*i*) ClustalX for the sequence alignment with the template A_{2A}AR (PDB code 3EML) [3], (*ii*) Modeler for the generation and selection of homology models and loop refinement procedures [26], (*iii*) Molprobity [35] and PDB2PQR [36] servers for the assessment of Asn/Gln/His rotamers, and side chain protonation states, and finally (*iv*) tools from Schrödinger Suite for energetic structural refinements [37]. Steps (*iii*) and (*iv*) were performed also for the refinement of the crystal structure of A_{2A}AR (PDB code 3EML).

Molecular dockings were performed with GOLD v4 software [27]. A sphere of 15 Å was centered in the C-γ of the conserved residue Ile 7.39, ensuring a proper search grid in the binding site of the receptor. 20 genetic algorithm runs were performed for each ligand,

employing ChemScore as scoring function, and allowing rotation of the protein hydroxyl groups. For the A_{2A}AR structure, additional side chain rotamers at residues Glu 5.30 and His 7.29 were considered, taking into account the induced-fit effect observed in the crystal structure of A_{2A}AR in complex with a relatively similar chemical scaffold, the 1,2,4-triazine derivative [34] (PDB code 3UZC). Fig. 3 was prepared with PyMOL v1.2, including the structural superimposition of A_{2A}AR and A_3AR ('super' command) and the calculation of Connolly surfaces of their binding sites with the default 1.4 Å probe.

7.1.2. 3D-QSAR

The software Pentacle [29] was employed for the generation of 3D-QSAR models (see Table 1) following previously published procedures by us [20]. The model originally reported in ref. [9] (*model I*) was extended with the tested molecules in that same effort (*model II*), and used with predictive purposes in this work (see Figs. 2 and 4A). Finally, a partial least squares model considering all diaryl-pyrimidines that found satisfactory binding modes on A_3AR (*model III*) was built in order to extract the main pharmacophoric elements of the series (Fig. 4B). The common methodology employed in these 3D-QSAR models includes four consecutive stages, where we used default options unless specified: (*i*) computation of the molecular interaction fields (MIFs) with selected chemical probes from the GRID force field, in the present case DRY, O, N1 and TIP probes, (*ii*) discretization of the MIFs with the AMANDA algorithm [28], (*iii*) consistency large auto and cross correlation (CLACC), which guarantees that a given variable represents exactly the same information for every compound of the series, in this case generated based on the biological superimposition of the ligands using the "strict" options, and (*iv*) two rounds of fractional factorial design were applied for the selection of the most relevant variables in the model.

7.2. Chemistry

Commercially available starting materials, reagents and solvents were purchased (Sigma–Aldrich) and used without further purification. After extraction from aqueous phases, the organic solvents were dried over anhydrous sodium sulfate. The reactions were monitored by thin-layer chromatography (TLC) with 2.5 mm Merck silica gel GF 254 strips, and the purified compounds each showed a single spot; unless stated otherwise, UV light and/or iodine vapor were used for detection of compounds. The Suzuki cross-coupling reactions were performed in coated Kimble vials on a PLS (6 × 4) Organic Synthesiser with orbital stirring. Purity and identity of all tested compounds were established by a combination of HPLC, mass spectrometry and NMR spectra. Purification of isolated products was carried out by column chromatography (Kieselgel 0.040–0.063 mm, E. Merck) or medium pressure liquid chromatography (MPLC) on a CombiFlash Companion (Teledyne ISCO) with RediSep pre-packed normal-phase silica gel (35–60 μm) columns followed by recrystallization. Melting points were determined on a Gallenkamp melting point apparatus and are uncorrected. The NMR spectra were recorded on Bruker AM300 and XM500 spectrometers. Chemical shifts are given as δ values against tetramethylsilane as internal standard and *J* values are given in Hz. Mass spectra were obtained on a Varian MAT-711 instrument. High resolution mass spectra were obtained on an Autospec Micromass spectrometer. Analytical HPLC was performed on an Agilent 1100 system using an Agilent Zorbax SB-Phenyl, 2.1 mm × 150 mm, 5 μm column with gradient elution using the mobile phases (A) H_2O containing 0.1% CF_3COOH and (B) MeCN and a flow rate of 1 mL/min. The purity of all tested compounds was determined to be >95%. Acetylation of 4-amino-2,6-dichloropyrimidine (**1**) was near quantitative (97%).

7.2.1. General procedure for the synthesis of compounds **4**

A mixture of the amide **2** (0.43 mmol), boronic acids **3** (1.3 mmol), $Pd(PPh_3)_4$ (0.043 mmol), and Na_2CO_3 (2.1 mmol) in 5 mL of a mixture of DME/$H_2$0 (3:1) in coated Kimble vials was stirred with orbital stirring at 110 °C for 12 h. The resulting mixture was concentrated in vacuo and then ethyl acetate was added. This solution was washed with water and NaOH 1 N to remove the acid boronic excess. The organic layer was collected, dried over Na_2SO_4, filtered and concentrated in vacuo. The residue was purified by column chromatography or preparative method on silica gel.

7.2.2. N-(2,6-Bis(3-methoxyphenyl)pyrimidin-4-yl)acetamide (**4c**)

Yield: 93%. Mp 135–136 °C. ^{1}H NMR ($CDCl_3$) δ (ppm): 2.14 (3H, s, CH_3), 3.86 (3H, s, OCH_3), 3.89 (3H, s, OCH_3), 7.00–7.05 (2H, m, Aromatics), 7.38 (2H, q, *J* = 7.8 Hz, Aromatics), 7.78 (2H, q, *J* = 7.8 Hz, Aromatics), 8.02–8.09 (2H, m, Aromatics), 8.47 (1H, s, NH), 8.68 (1H, s, H_5). ^{13}C NMR ($CDCl_3$) δ (ppm): 169.6, 165.6, 163.5, 159.8, 159.7, 158.2, 138.7, 138.4, 129.7, 129.4, 120.5, 119.8, 116.7, 116.4, 112.9, 112.6, 103.3, 55.29, 55.23, 24.7. MS *m*/*z*: 350 (MH^+) (100). HRMS (ESI) calculated for $C_{20}H_{20}N_3O_3$ 350.1426, found 350.1492.

7.2.3. N-(2,6-Bis(4-(trifluoromethoxy)phenyl)pyrimidin-4-yl) acetamide (**4e**)

Yield: 81%. Mp 146–147 °C. ^{1}H NMR ($CDCl_3$) δ (ppm): 2.31 (3H, s, CH_3), 7.31–7.37 (4H, t, *J* = 8.2 Hz, Aromatics), 8.07 (1H, s, NH), 8.26 (2H, d, *J* = 8.7 Hz, Aromatics), 8.50–8.54 (3H, m, 2H Aromatics + 1H, H_5). ^{13}C NMR ($CDCl_3$) δ (ppm): 169.3, 164.4, 162.6, 158.2, 151.1, 151.0, 148.0, 147.5, 135.5, 135.3, 129.6, 128.9, 120.8, 120.4, 103.0, 24.8. MS *m*/*z*: 458 (MH^+) (100). HRMS (ESI) calculated for $C_{20}H_{14}F_6N_3O_3$ 458.0861, found 458.0938.

7.2.4. N-(2,6-bis(4-ethoxyphenyl)pyrimidin-4-yl)acetamide (**4f**)

Yield: 76%. Mp 155–156 °C. ^{1}H NMR ($CDCl_3$) δ (ppm): 1.44 (6H, t, *J* = 6.7 Hz, 2× CH_2CH_3), 2.17 (3H, s, CH_3), 4.11 (4H, q, *J* = 6.7 Hz, 2× CH_2CH_3), 6.95–7.01 (4H, m, Aromatics), 8.20 (2H, d, *J* = 8.6 Hz, Aromatics), 8.36–8.43 (4H, m, 2H Aromatics + 1H H_5 + 1H NH). ^{13}C NMR ($CDCl_3$) δ (ppm): 169.4, 165.2, 163.4, 161.2, 161.1, 157.9, 129.9, 129.6, 129.4, 128.8, 114.4, 114.1, 101.2, 63.4, 24.7, 14.6. MS *m*/*z*: 378 (MH^+) (100). HRMS (ESI) calculated for $C_{22}H_{24}N_3O_3$ 378.1739, found 378.1818.

7.2.5. N-(2,6-Bis(4-methoxystyryl)pyrimidin-4-yl)acetamide (**4g**)

Yield: 37%. Mp 134–135 °C. ^{1}H NMR ($CDCl_3$) δ (ppm): 2.24 (3H, s, CH_3), 3.84 (6H, s, 2× OCH_3), 6.93 (4H, d, *J* = 8.1 Hz, Aromatics), 7.01 (2H, dd, *J* = 16.15 Hz, *J* = 4.65 Hz, CH=CH), 7.55 (4H, d, *J* = 8.3 Hz, Aromatics), 7.88 (2H, dd, *J* = 15.9 Hz, *J* = 5.07 Hz, CH=CH), 7.96 (1H, s, H_5), 8.09 (1H, s, NH). ^{13}C NMR ($CDCl_3$) δ (ppm): 169.4, 164.5, 164.0, 160.4, 160.3, 157.3, 137.5, 137.4, 136.3, 129.0, 128.9, 128.6, 128.5, 124.9, 124.1, 114.1, 103.9, 55.2, 55.1, 24.8. MS *m*/*z*: 402 (MH^+) (100). HRMS (ESI) calculated for $C_{24}H_{24}N_3O_3$ 402.1739, found 402.1815 (M^+).

7.2.6. N-(2,6-Bis(2,3-dimethoxyphenyl)pyrimidin-4-yl)acetamide (**4h**)

Yield: 76%. Mp 105–106 °C. ^{1}H NMR ($CDCl_3$) δ (ppm): 2.19 (3H, s, CH_3), 3.86–3.93 (12H, m, 4× OCH_3), 7.03 (2H, d, *J* = 6.7 Hz, Aromatics), 7.13 (2H, t, *J* = 7.8 Hz, Aromatics), 7.30 (1H, d, *J* = 7.8 Hz, Aromatics), 7.55 (1H, d, *J* = 7.8 Hz, Aromatics), 8.31 (1H, s, NH), 8.63 (1H, s, H_5). ^{13}C NMR ($CDCl_3$) δ (ppm): 169.2, 164.6, 164.4, 157.2, 153.2, 153.0, 148.0, 147.5, 133.6, 132.0, 123.8, 122.6, 122.4, 114.0, 113.5, 107.6, 61.5, 61.1, 55.9, 24.6. MS *m*/*z*: 409 (98). HRMS (EI) calculated for $C_{22}H_{23}N_3O_5$ 409.1638, found 409.1651.

7.2.7. N-(2,6-Bis(2,5-dimethoxyphenyl)pyrimidin-4-yl)acetamide (**4j, ISVY350**)

Yield: 57%. Mp 176–177 °C. ^{1}H NMR ($CDCl_3$) δ (ppm): 2.10 (3H, s, CH_3), 3.77–3.90 (12H, m, 4× OCH_3), 6.96 (4H, s, Aromatics), 7.32

(1H, s, Aromatics), 7.66 (1H, s, Aromatics), 8.72 (2H, s, 1H, H_5 + 1H, NH). ^{13}C NMR ($CDCl_3$) δ (ppm): 169.6, 164.2, 157.2, 153.5, 153.4, 152.3, 151.7, 128.9, 127.1, 117.1, 116.5, 116.2, 115.7, 113.4, 112.8, 108.1, 56.3, 56.1, 55.7, 24.3. MS *m*/*z*: 410 (MH^+) (100). HRMS (ESI) calculated for $C_{22}H_{24}N_3O_5$ 409.1638, found 410.1702.

*7.2.8. N-(2,6-Bis(2,6-dimethoxyphenyl)pyrimidin-4-yl)acetamide (**4k**)*

Yield: 27%. Mp 184–185 °C. ^{1}H NMR ($CDCl_3$) δ (ppm): 1.97 (3H, s, CH_3), 3.67 (6H, s, 2× OCH_3), 3.72 (6H, s, 2× OCH_3), 6.57–6.59 (4H, m, Aromatics), 7.27 (2H, s, Aromatics), 8.06 (1H, s, H_5), 9.08 (1H, s, NH). ^{13}C NMR ($CDCl_3$) δ (ppm): 169.5, 165.4, 163.8, 161.2, 160.7, 159.2, 138.9, 138.7, 106.2, 105.8, 103.6, 103.4, 103.1, 55.40, 55.36, 24.7. MS *m*/*z*: 410 (MH^+) (100). HRMS (ESI) calculated for $C_{22}H_{24}N_3O_5$ 410.1638, found 410.1717.

*7.2.9. N-(2,6-Bis(3,4-dimethoxyphenyl)pyrimidin-4-yl)acetamide (**4l**, **ISVY345**)*

Yield: 85%. Mp 147–148 °C. ^{1}H NMR ($CDCl_3$) δ (ppm): 2.26 (3H, s, CH_3), 3.96 (6H, s 2× OCH_3), 4.00 (6H, s, 2× OCH_3), 6.98 (2H, d, J = 8.4 Hz, Aromatics), 7.82 (1H, d, J = 8.4 Hz, Aromatics), 7.86 (1H, s, Aromatics), 8.05 (1H, s, Aromatics), 8.12 (1H, d, J = 8.4 Hz, Aromatics), 8.26 (1H, s, NH), 8.39 (1H, s, H_5). ^{13}C NMR ($CDCl_3$) δ (ppm): 169.4, 165.2, 163.2, 157.8, 151.3, 151.2, 148.9, 148.6, 130.1, 129.8, 121.3, 120.6, 110.7, 110.5, 109.9, 109.8, 101.6, 55.8, 55.7, 24.8. MS *m*/*z*: 410 (MH^+) (100). HRMS (ESI) calculated for $C_{22}H_{24}N_3O_5$ 410.1638, found 410.1710.

*7.2.10. N-(2,6-Bis(3,5-dimethoxyphenyl)pyrimidin-4-yl)acetamide (**4n**)*

Yield: 98%. Mp 186–187 °C. ^{1}H NMR ($CDCl_3$) δ (ppm): 2.27 (3H, s, CH_3), 3.89 (12H, s, 4× OCH_3), 6.61 (2H,s, Aromatics), 7.38 (2H, s, Aromatics), 7.67 (2H, s, Aromatics), 8.13 (1H, s, NH), 8.45 (1H, s, H_5). ^{13}C NMR ($CDCl_3$) δ (ppm): 169.4, 165.5, 163.2, 160.9, 160.7, 158.0, 139.3, 139.1, 105.8, 105.3, 103.4, 103.2, 102.8, 55.39, 55.34, 24.7. MS *m*/*z*: 409 (72). HRMS (EI) calculated for $C_{22}H_{23}N_3O_5$ 409.1638, found 409.1642.

*7.2.11. N-(2,6-Bis(3,4,5-trimethoxyphenyl)pyrimidin-4-yl) acetamide (**4o**)*

Yield: 95%. Mp 199–200 °C. ^{1}H NMR ($CDCl_3$) δ (ppm): 2.30 (3H, s, CH_3), 3.93 (6H, s, 2× OCH_3), 3.98 (12H, s, 4× OCH_3), 7.48 (2H, s, Aromatics), 7.79 (2H, s, Aromatics), 8.15 (1H, s, NH), 8.42 (1H, s, H_5). ^{13}C NMR ($CDCl_3$) δ (ppm): 169.4, 165.2, 163.0, 158.0, 153.3, 153.0, 140.4, 132.5, 132.4, 105.1, 105.0, 104.4, 104.3, 102.4, 60.8, 56.0, 55.9, 24.8. MS *m*/*z*: 469 (100). HRMS (EI) calculated for $C_{24}H_{27}N_3O_7$ 469.1849, found 469.1852.

Acknowledgments

This work has been developed in the frame of the Red Gallega de Investigación y Desarrollo de Medicamentos (REGID) and was financially supported by the Ministerio de Ciencia e Innovación (MICINN grant SAF2011-30104) and the Xunta de Galicia (09CSA016234PR). D.R. is recipient of a predoctoral grant from the Fondo de Investigación en Salud (ISCIII). H.G.T. and A.C. are researchers of the Isidro Parga Pondal program (Xunta de Galicia, Spain).

References

[1] B.B. Fredholm, A.P. Ijzerman, K.A. Jacobson, J. Linden, C.E. Muller, Pharmacol. Rev. 63 (2011) 1–34.
[2] K.A. Jacobson, Z.-G. Gao, Nat. Rev. Drug Discov. 5 (2006) 247–264.
[3] V.-P. Jaakola, M.T. Griffith, M.A. Hanson, V. Cherezov, E.Y.T. Chien, J.R. Lane, A.P. Ijzerman, R.C. Stevens, Science 322 (2008) 1211–1217.
[4] J. Linden, Trends Pharmacol. Sci. 15 (1994) 298–306.
[5] B.T. Liang, K.A.A. Jacobson, Proc. Natl. Acad. Sci. U. S. A. 9 (1998) 6995–6999.
[6] R. Akkari, J.C. Burbiel, J. Hockemeyer, C.E. Müller, Curr. Top. Med. Chem. 6 (2006) 1375–1399.
[7] C.H. Mitchell, K. Peterson-Yantorno, D.A. Carré, A.M. McGlinn, M. Coca-Prados, R.A. Stone, M.M. Civan, Am. J. Physiol. 276 (1999) 659–666.
[8] P.G. Baraldi, M.A. Tabrizi, R. Romagnoli, F. Fruttarolo, S. Merighi, K. Varani, S. Gessi, P.A. Borea, Curr. Med. Chem. 12 (2005) 1319–1329.
[9] S. Gessi, E. Cattabriga, A. Avitabile, R. Gafà, G. Lanza, L. Cavazzini, N. Bianchi, R. Gambari, C. Feo, A. Liboni, S. Gullini, E. Leung, S. Mac-Lennan, P.A. Borea, Clin. Cancer Res. 10 (2004) 5895–5901.
[10] P. Fishman, S. Bar-Yehuda, Curr. Top. Med. Chem. 3 (2003) 463–469.
[11] S. Gessi, S. Merighi, K. Varani, E. Leung, S.M. Lennan, P.A. Bore, Pharmacol. Ther. 117 (2008) 123–140.
[12] K.A. Jacobson, A.M. Klutz, D.K. Tosh, A.A. Ivanov, D. Preti, P.G. Baraldi, Medicinal chemistry of the A_3 adenosine receptor: agonists, antagonists, and receptor engineering, adenosine receptors in health and disease, in: B.B. Fredholm (Ed.), Handbook of Experimental Pharmacology, vol. 193, Springer, 2009, pp. 123–159.
[13] P.G. Baraldi, D. Preti, P.A. Borea, K. Varani, J. Med. Chem. 55 (2012) 5676–5703.
[14] P.G. Baraldi, M.A. Tabrizi, F. Fruttarolo, A. Bovero, B. Avitabile, D. Preti, R. Romagnoli, S. Merighi, S. Gessi, K. Varani, P.A. Borea, Drug Dev. Res. 58 (2003) 315–329.
[15] F. Luan, F. Borges, M.N.D.S. Cordeiro, Curr. Top. Med. Chem. 12 (2012) 878–894.
[16] K. Nieber, A. Lewerenz, S. Hentschel, Z. Vissiennon, Bioforum 25 (2002) 237–240.
[17] T.W. Stone, Adv. Exp. Med. Biol. 513 (2002) 249–280.
[18] S. Merighi, P. Mirandola, K. Varani, S. Gessi, S. Capitani, E. Leung, P.G. Baraldi, M.A. Tabrizi, P.A. Borea, Biochem. Pharmacol. 66 (2003) 739–748.
[19] P.G. Baraldi, M.A. Tabrizi, S. Gessi, P.A. Borea, Chem. Rev. 108 (2008) 238–263.
[20] V. Yaziji, D. Rodriguez, H. Gutierrez-de-Teran, A. Coelho, O. Caamano, X. Garcia-Mera, J. Brea, M.I. Loza, M.I. Cadavid, E. Sotelo, J. Med. Chem. 54 (2011) 457–471.
[21] L.C.W. Chang, R.F. Spanjersberg, J.K. von Kuenzel, T. Mulder-Krieger, G. van den Hout, M.W. Beukers, J. Brussee, A.P. Ijzerman, J. Med. Chem. 47 (2004) 6529–6540.
[22] B. Cosimelli, G. Greco, M. Ehlardo, E. Novellino, F. Da Settimo, S. Taliani, C. La Motta, M. Bellandi, T. Tuccinardi, A. Martinelli, O. Ciampi, M.L. Trincavelli, C. Martini, J. Med. Chem. 51 (2008) 1764–1770.
[23] K.Y. Jung, S.K. Kim, Z.G. Gao, A.S. Gross, N. Melman, K.A. Jacobson, Y.C. Kim, Bioorg. Med. Chem. 12 (2004) 613–623.
[24] O. Lenzi, V. Colotta, D. Catarzi, F. Varano, G. Filacchioni, C. Martini, L. Trincavelli, O. Ciampi, K. Varani, F. Marighetti, E. Morizzo, S. Moro, J. Med. Chem. 49 (2006) 3916–3925.
[25] S. Taliani, C. La Motta, L. Mugnaini, F. Simorini, S. Salerno, A.M. Marini, F. Da Settimo, S. Cosconati, B. Cosimelli, G. Greco, V. Limongelli, L. Marinelli, E. Novellino, O. Ciampi, S. Daniele, M.L. Trincavelli, C. Martini, J. Med. Chem. 53 (2010) 3954–3963.
[26] A. Sali, T.L. Blundell, J. Mol. Biol. 234 (1993) 779–815.
[27] M.L. Verdonk, J.C. Cole, M.J. Hartshorn, C.W. Murray, R.D. Taylor, Proteins – Struct. Funct. Genet. 52 (2003) 609–623.
[28] A. Duran, G.C. Martinez, M. Pastor, J. Chem. Inf. Model. 48 (2008) 1813–1823.
[29] Pentacle 1.1, Molecular Discovery, Ltd, Perugia, Italy, 2009.
[30] V. Yaziji, A. Coelho, A. El Maatougui, J. Brea, M.I. Loza, X. García-Mera, E. Sotelo, J. Comb. Chem. 11 (2009) 519–522.
[31] N. Miyara, T. Yanagi, A. Suzuki, Synth. Commun. 11 (1981) 513–519.
[32] M.P. Bosch, F. Campos, I. Niubo, G. Rosell, J.L. Diaz, J. Brea, M.I. Loza, A. Guerrero, J. Med. Chem. 47 (2004) 4041–4053.
[33] J.A. Ballesteros, H. Weinstein, Methods Neurosci. 25 (1995) 366–428.
[34] M. Congreve, S.P. Andrews, A.S. Dore, K. Hollenstein, E. Hurrell, C.J. Langmead, J.S. Mason, I.W. Ng, B. Tehan, A. Zhukov, M. Weir, F.H. Marshall, J. Med. Chem. 55 (2012) 1898–1903.
[35] I.W. Davis, A. Leaver-Fay, V.B. Chen, J.N. Block, G.J. Kapral, X. Wang, L.W. Murray, W.B. Arendall, J. Snoeyink, J.S. Richardson, D.C. Richardson, Nucleic Acids Res. 35 (2007) W375–W383.
[36] T.J. Dolinsky, J.E. Nielsen, J.A. McCammon, N.A. Baker, Nucleic Acids Res. 32 (2004) W665–W667.
[37] Schrödinger, L.L.C., New York, NY, 2009.